

The Catalase Activity of Catalase-Peroxidases Is Modulated by Changes in the pK_a of the Distal Histidine

Miguel Machuqueiro^{1b}

Centro de Química e Bioquímica, Departamento de Química e Bioquímica, Faculdade de Ciências, Universidade de Lisboa, 1749-016 Lisboa, Portugal

Bruno Victor

Centro de Química e Bioquímica, Departamento de Química e Bioquímica, Faculdade de Ciências, Universidade de Lisboa, 1749-016 Lisboa, Portugal

Jacek Switala

Department of Microbiology, University of Manitoba, Winnipeg, MB R3T 2N2, Canada

Jacylyn Villanueva

Department of Microbiology, University of Manitoba, Winnipeg, MB R3T 2N2, Canada

Carne Rovira^{1b}

Departament de Química Orgànica and Institut de Química Teòrica i Computacional (IQTCUB), Universitat de Barcelona, Martí i Franquès 1, 08028 Barcelona, Spain

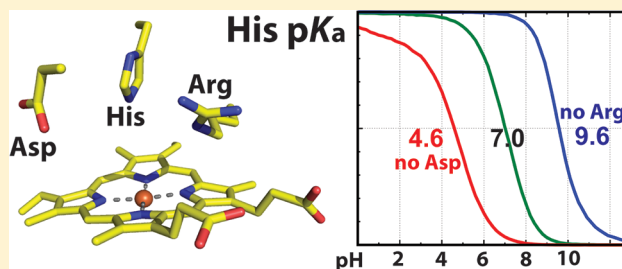
Ignacio Fita

Institut de Biologia Molecular de Barcelona (CSIC), Parc Científic de Barcelona, Baldiri i Reixac 10-12, 08028 Barcelona, Spain

Peter C. Loewen^{*1b}

Department of Microbiology, University of Manitoba, Winnipeg, MB R3T 2N2, Canada

ABSTRACT: The unusual Met-Tyr-Trp adduct composed of cross-linked side chains along with an associated mobile Arg is essential for catalase activity in catalase-peroxidases. In addition, acidic residues in the entrance channel, in particular an Asp and a Glu ~ 7 and ~ 15 Å, respectively, from the heme, significantly enhance catalase activity. The mechanism by which these channel carboxylates influence catalase activity is the focus of this work. Seventeen new variants with fewer and additional acidic residues have been constructed and characterized structurally and for enzymatic activity, revealing that their effect on activity is roughly inversely proportional to their distance from the heme and adduct, suggesting that the electrostatic potential of the heme cavity may be affected. A discrete group of protonable residues are contained within a 15 Å sphere surrounding the heme iron, and a computational analysis reveals that the pK_a of the distal His₁₁₂, alone, is modulated within the pH range of catalase activity by the remote acidic residues in a pattern consistent with its protonated form having a key role in the catalase reaction cycle. The electrostatic potential also impacts the catalytic reaction through its influence on the charged status of the Met-Tyr-Trp adduct.



Catalase-peroxidases or KatGs are fascinating proteins with a peroxidase-like core, catalyzing a broad substrate-range peroxidase reaction, that have evolved to support a robust catalase

Received: December 19, 2016

Revised: March 15, 2017

Published: April 14, 2017

reaction, dismutating hydrogen peroxide to oxygen and water,¹ and an oxygenase function that generates superoxide.^{2–4} The *in vivo* roles of the peroxidase and oxidase reactions are as yet undefined. Furthermore, a combination of the oxygenase and peroxidase reactions of KatG in *Mycobacterium tuberculosis* facilitates the conversion of the prodrug isoniazid into isonicotinyl-NAD, an active anti-tubercular drug.⁵

Rationalizing the overlapping mechanisms of these seemingly disparate reactions has been a challenge. The key lies in a unique intramolecular adduct of the cross-linked side chains of Met₂₆₄, Tyr₂₃₈, and Trp₁₁₁ [residue numbering corresponds to that of *Burkholderia pseudomallei* KatG (BpkatG)], hereafter termed the M-Y-W adduct, its reversible association with a mobile Arg₄₂₆, and a reversible perhydroxy modification on the indole of the M-Y-W adduct (M-Y-W₁₁₁-OOH), with two orientations, A and B, all in the proximity of the heme (Figure 1). Computational

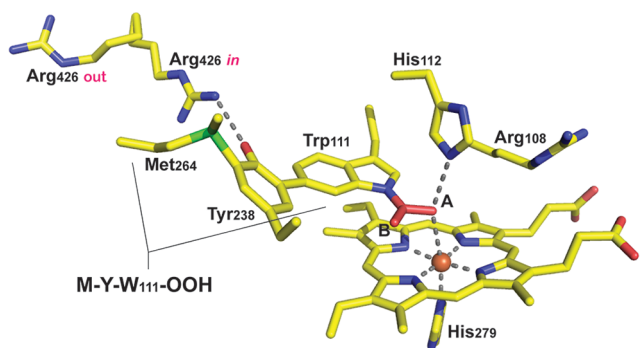


Figure 1. Orientation of the key residues surrounding the heme in BpKatG. The side chains of the three residues, Met₂₆₄, Tyr₂₃₈, and Trp₁₁₁, are cross-linked to form the M-Y-W adduct that can be reversibly perhydroxylated on the indole nitrogen of Trp₁₁₁ to create the M-Y-W₁₁₁-OOH modification. The terminal -OH of the perhydroxy modification is found in two orientations, A, in contact with the heme iron and His₁₁₂, and B, having no interactions in the protein. The mobile Arg₄₂₆ can also adopt two conformations, *in*, forming an ionic interaction with a tyrosinate ion on Tyr₂₃₈, and *out*, rotated away from the adduct.

studies have implicated the transient formation of a radical on the M-Y-W adduct⁶ as a possible intermediate in the catalytic reaction and in the reversible formation of the M-Y-W₁₁₁-OOH modification.^{7,8} In addition, electron paramagnetic resonance (EPR) studies have identified two sites of stable radical accumulation, Trp₁₃₉ and Trp₁₅₃,⁹ thereby defining a possible electron transfer pathway from isoniazid to the M-Y-W adduct and heme for the generation of superoxide, required for isoniazid activation.^{9,10}

A comprehensive mechanism (Figure 2) for the catalytic process has been proposed,^{8,11,12} and while the process is cyclic, a starting point is defined at RS 1 (resting state 1), the predominant species that accumulates in protein crystals actively metabolizing H₂O₂.⁸ RS 1 must be converted to RS 2, with the release of O₂, before H₂O₂ can bind for Compound I (Cpd I) formation. The subsequent reduction of Cpd I may in fact be concerted, but discrete intermediates are shown to define more clearly the molecular changes. A transient radical is formed on the M-Y-W adduct with the transfer of an electron to the porphyrin (I_A), followed by the binding of H₂O₂ to Cpd I (I_B). The transfer of a hydrogen atom to the ferryl-oxo species yields a two-radical ferryl-hydroxo intermediate (I_C), and the transfer of a proton from the Trp₁₁₁ indole produces water, leaving the two radicals (I_D) to combine into RS 1. All species in this cycle

have been characterized by either X-ray crystallography or quantum mechanical/molecular mechanical calculations.

Despite this detailed understanding of the inner workings of KatGs, a perplexing question regarding the influence of acidic residues on catalase activity remains. Removal of an aspartate side chain ~7 Å from the heme iron (Asp₁₄₁ in Figure 3) reduces catalase activity by >95% with little change in peroxidase activity.^{13,14} Even more surprising is the fact that removal of a glutamate side chain ~15 Å from the heme iron (Glu₂₄₂ in Figure 3) reduces catalase activity by >70%.¹⁵ An electrical potential between the negatively charged carboxylate and a positively charged iron, previously proposed in classical catalases,¹⁶ was suggested as a possible explanation,¹⁵ but restoration of catalase activity in the D141A/R108A double variant suggested a more complex situation.¹⁴

In this paper, we confirm the importance of channel carboxylates for the catalase activity of catalase-peroxidases with a combination of crystallographic, computational, and biochemical approaches and demonstrate that native enzyme activity can actually be enhanced by the introduction of additional carboxylates in the entrance channel. Seventeen new BpKatG variants with changes in channel residues are characterized biochemically and structurally to demonstrate the scope of the carboxylate influence. In parallel, the pK_a values for all ionizable residues in the protein are calculated revealing a correlation among increasing numbers of channel carboxylates, increasing His₁₁₂ pK_a, and catalase activity. The impact of these results on the catalase reaction mechanism is discussed.

EXPERIMENTAL PROCEDURES

Chemicals and Media. All chemicals were obtained from Sigma-Aldrich or Fisher unless otherwise stated. All components of media were obtained from Becton-Dickson, and all restriction enzymes were obtained from Invitrogen.

Enzyme Assays. Catalase activity was determined by the method of Rørth and Jensen¹⁷ in a Gilson oxygraph equipped with a Clark electrode. One unit of catalase is defined as the amount that decomposes 1 μmol of H₂O₂ in 1 min in a 60 mM H₂O₂ solution at pH 7.0 and 37 °C. Peroxidase activity was determined using ABTS [2,2'-azinobis(3-ethylbenzothiazoline)-sulfonic acid] (ε₄₀₅ = 36800 M⁻¹ cm⁻¹),¹⁸ and one unit is defined as the amount that decomposes 1 μmol of ABTS in a solution of 0.4 mM ABTS and 2.5 mM hydrogen peroxide at pH 4.5 and 25 °C.¹⁹ Assays were performed in triplicate and results averaged.

Variant Protein Construction, Purification, and Characterization. The following oligonucleotides were purchased from Invitrogen and used to mutate pBpG-KC, containing the *KpnI*-*Clal* fragment (base pairs 1–1006 of BpKatG), or pBpCH, containing the *Clal*-*HindIII* fragment (base pairs 1003–1731), following the Kunkel²⁰ procedure: CCCGACAA-CGACAACCTCGAC (A143D), AAGACTCTGGACGAACCT-GAGC (L209D), ATCTGGCTGCAACTGAGCGGC (E210Q), CTGGCTGGAAGACAGCGCGGC (L211D), GCCGCCGTGGAGATGGGCCTCA (Q233E), CAGATGG-GCCGACTCTACGTGA (L236D), ATCTACGTGAGATCG-GAAGGCC (N240D), TGAATCCGGCAAGCCCGGTGC (E242Q), GCGGGGCCGACTCGAACGTC (A290D), GCGTCAACGACGGCGCCGAG (V293D), GTCGGCGC-CGCGCCGAGGCC (E296A), ACGAGCGGGACGAAG-TCACG (L326D), GAAGAGCCCGGACGGCGCGCACCC (A357D), and CCGGCGGGCGACCACCAGTGG (A359D). The mutant sequences were confirmed and used to generate plasmids pA143D, pL209D, pE210Q, pL211D, pQ233E, pL236D,

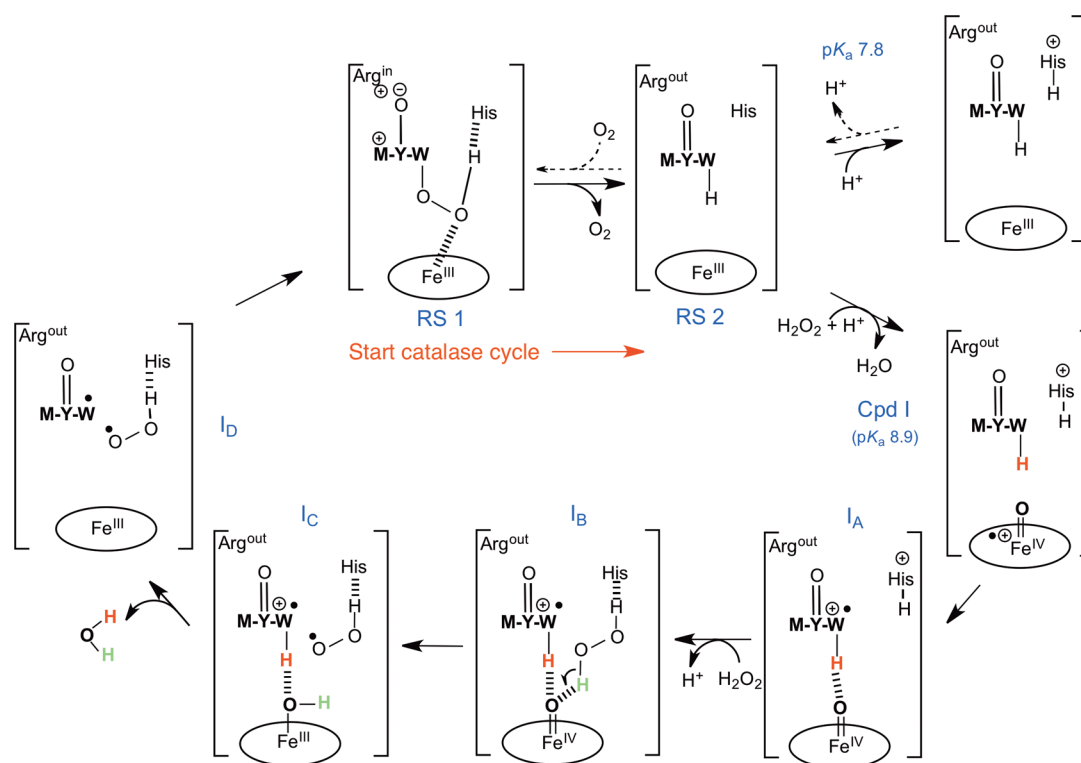


Figure 2. Catalase reaction scheme originally proposed in ref 8 but modified to include the possible roles of distal His₁₁₂ protonation. RS 1 predominates in the crystal structure, suggesting an energy barrier for O₂ removal to generate RS 2 and Cpd I formation. For the purposes of discussion, we have indicated that the catalase cycle begins with RS 1.

pN240D, pE242Q, pA290D, pV293D, pE296A, pL326D, pA357D, pA359D, and pQ233E/N240D by reincorporating the fragment into the full-length *katG* gene. Plasmid pD141A has been constructed previously¹⁴ and was used for the construction of multiple-variant plasmids pD141A/Q233E and D141A/Q233E/N240D. The native and variant proteins were expressed and purified as described previously.⁹

Crystallization of the KatG Variants. Crystals were obtained at room temperature by the vapor diffusion hanging drop method at 20 °C over a reservoir solution containing 16–20% (w/v) PEG 4000, 20% 2-methyl-2,4-pentandiol, and 0.1 M sodium citrate (pH 5.6).^{10,21} Crystals were in primitive orthorhombic space group $P2_12_12_1$ with two subunits in the crystal asymmetric unit. Diffraction data were collected using synchrotron beamline CMCF 08ID-1 at the Canadian Light Source in Saskatoon, SK, from crystals flash-cooled in reservoir buffer and cooled with a nitrogen cryostream. Data were processed and scaled using XDS²² and SCALA²³ (Table 1). The structural refinement starting with the native BpKatG structure [Protein Data Bank (PDB) entry 1MWV] was completed using REFMAC²⁴ and manual modeling with the molecular graphics program COOT.²⁵ Figures were generated using PYMOL (The PYMOL Molecular Graphics System, Schrodinger, LLC). The cavities associated with the main channel were visualized with HOLLOW.²⁶

pK_a Calculations. The distribution of all charged or potentially charged residues in KatG was mapped, revealing the isolation of a subset of charged side chains in the heme cavity (Figure 4). A summation of the charges within the heme vicinity (Figure 4 C) reveals a net negative charge. A sphere of 15 Å centered at the heme iron contains only the charged side chains implicated in the catalytic mechanism or interacting with the heme, the Lys₂₈₃-Glu₃₂₇ pair, and Glu₂₄₂. The mobile Arg₄₂₆ is

outside the sphere when in the out (or R)²⁷ conformation and inside the sphere when in the in (or Y)²⁷ conformation interacting with the adduct Tyr₂₃₈, which requires the tyrosine to be unprotonated. The pK_a changes in the side chains of all residues found in this ~15 Å coordination sphere of the iron atom of native BpKatG and its D141A, E242Q, Q233E, and N240D variants were calculated at different stages of the catalytic cycle, including resting state 1 [RS 1 with Fe^{III} and W₁₁₁-OOH (Figure 2)], resting state 2 (RS 2 with Fe^{III} and M-Y-W₁₁₁-H), Compound I (with Fe^{IV}=O and W₁₁₁-H), and in the presence of acetate. In addition, both RS 1 and RS 2 were considered with Tyr₂₃₈ in its neutral hydroxyl form and in its anionic form, with and without interaction with the mobile Arg₄₂₆. The structures for each state were derived from crystal structures, including RS 1 of native BpKatG from 5SXR (3N3O),¹⁰ D141A from 5SYH (4KAS),²⁸ D141A with acetate bound from 5KSF, E242Q from 5SYU (4QZK), S324T from 5L02 (1X7U),²⁹ Q233E from 5SYW (4QZN), N240D from 5SYV (4QZL), BpKatG Cpd I from 5SW8 (2B2R),²⁷ D141A Cpd I, generated *in silico* from 5SYH and 5SW8, and RS 2 of BpKatG from 5SXS (3N3P).¹⁰ The first 14 residues of all BpKatG structures are not resolved and were not included in the calculations.

The charge parameters were taken from a previous work.³⁰ For M-Y-W₁₁₁-OOH, we started with the coordinates from 5SXR (3N3O)¹⁰ and the geometry was optimized with the wb97X functional³¹ and the 6-31+G** basis set. The electrostatic potentials were calculated on the optimized conformations following a previous protocol.³⁰ The parameters for acetic acid were easily derived from the side chains of aspartate or glutamate found in the Gromos 54a7 force field.^{32,33}

We used Poisson–Boltzmann (PB) calculations to compute the individual and pairwise terms needed to obtain the changes in

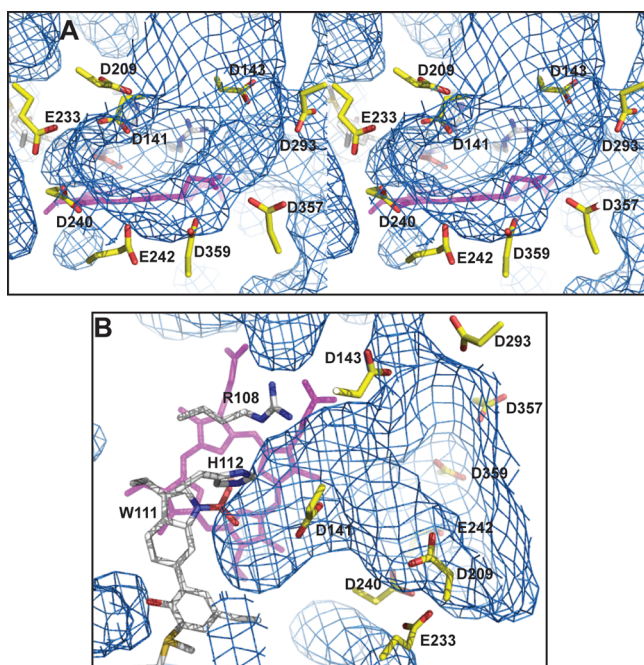


Figure 3. Distribution of carboxylates that enhance the catalase reaction. (A) Stereoview looking into the entrance channel illustrating the distribution around the opening. The heme is colored mauve for the sake of visibility. (B) View of the channel extending into the heme cavity looking down on the heme to illustrate the relative distances between the carboxylates and the heme. The locations of the various carboxylates are derived from the structures outlined in Table 1, including Asp₃₅₇ from SKQ2, Asp₃₅₉ from SKQ6, Asp₂₉₃ from SKQH, Asp₁₄₁ and Glu₂₄₂ from SLOS, Glu₂₃₃ from SSYW, and Asp₂₄₀ from SSYV. The location of the mutated side chain of L209D was fit *in silico*.

the free energies of protonation. These were then used to perform Monte Carlo (MC) sampling of the protonation states. pK_a values for protonable groups were obtained from the corresponding titration curves.³⁴ All calculations were performed considering alternative proton positions (tautomers) for all titratable sites.^{34,35} The atomic charges and radii used in the PB calculations were derived from the Gromos 54a7 force field,^{32,33} with the exception of the heme and M-Y-W peptide adduct, for which we used our QM-derived charges. All PB calculations consisted of finite-difference linear Poisson–Boltzmann calculations performed with MEAD,^{36,37} using a temperature of 300 K, an ionic strength of 100 mM, a molecular surface defined with a solvent probe radius of 1.4 Å,³⁸ and a Stern (ion exclusion) layer of 2.0 Å. A two-step focusing procedure³⁹ was used, with consecutive grid spacings of 1.0 and 0.25 Å. The dielectric constants of the solvent and protein were set to 80 and 20, respectively.³⁴ The value of 20 has been shown to minimize the error in pK_a predictions in a set of protein X-ray structures with known experimental pK_a values.³⁴ The MC simulations were performed using PETIT^{35,40} with multistate titrations by performing trial changes of both single and pair sites.^{35,40} MC simulations were performed at intervals of 0.2 pH unit, each using 10^5 MC cycles. Each cycle consisted of sequential state changes over all individual sites and also pairs of sites with at least one interaction term above 2.0 pK_a units.

For more details about pK_a calculations, please refer to refs 34 and 35. Reference 34 also provides a comprehensive study of pK_a values on several protein X-ray structures, which served as a benchmark for our methodology and revealed a typical error of ~ 0.8 pK unit.

RESULTS

Acidic Residues in the Entrance Channel Are Important for Catalase Activity. Mutation of acidic residues in the entrance channel of KatGs causes a decrease in catalase activity with little or no effect on peroxidase activity. For example, removal of the carboxylate of Asp₁₅₂ in *Synechocystis* KatG (SyKatG) or Asp₁₄₁ in BpKatG, ~ 7 Å from the heme iron, reduces activity by $>95\%$.^{13,14} A direct catalytic role of the carboxylate, although proposed,¹³ seemed unlikely because simultaneous removal of the nearby Arg₁₀₈ in the BpKatG double variant, D141A/R108A, returned catalytic activity to 80% of native levels.¹⁴ The alternative explanation that Asp₁₄₁ and Arg₁₀₈ were contributing to a charge balance in the heme cavity was proposed, although how the charges were influencing catalase activity was not clear. The puzzle of channel carboxylates deepened with the observation that removal of Glu₂₅₃ (Glu₂₄₂ in Figure 3) in SyKatG, situated 14 Å from the heme, reduced catalase activity by $\sim 70\%$.¹⁵ In this instance, an analogy was drawn with monofunctional catalases, where it was suggested that an electrical potential between an aspartate in the entrance channel and the heme acted on the electrical dipoles of incoming H₂O₂ to create a favorable or reactive orientation.¹⁶ However, the more open architecture of catalase-peroxidase entrance channels and the dramatic influence of Asp₁₄₁ suggested that other mechanisms should be considered.

To investigate further the role of channel carboxylates, a series of variants with acidic residues added and removed from various locations in the entrance channel have been constructed and characterized structurally (Table 1) and for activity (Table 2). Of the existing acidic residues, removal of Glu₂₁₀, Glu₂₉₆, and Glu₂₄₂ (see Figure 3 for location) causes a range of levels of inhibition, 20, 40, and 85%, respectively, roughly inversely correlated with their distance from the heme (24.1, 21.3, and 14.2 Å, respectively). Surprisingly, the insertion of additional acidic residues in a number of locations, including Gln₂₃₃ (to Glu) and Ala₁₄₃, Asn₂₄₀, Val₂₉₃, Ala₃₅₇, and Ala₃₅₉ (all to Asp), causes varying increases in catalase activity, again roughly inversely correlated with distance from the heme, although a 2-fold increase in activity is the maximum regardless of the number of carboxylates introduced. By contrast, replacement of Ala₂₉₀, Leu₂₃₆, and Leu₃₂₆ (all with Asp), the latter two within 12 Å of the heme, caused a small decrease in catalase activity for which an explanation is not obvious.

A survey of the location and orientation of the acidic residues relative to the cavity entrance and the heme (Figure 3) reveals that carboxylates in all quadrants surrounding the entrance are effective in causing activation. In other words, variations in activity (Table 2) could not be correlated with any changes in side chain location or water matrix in the entrance channel among the variants, including A143D (STXQ), A290D (SKQ0), A357D (SKQ2), A359D (SKQ6), V293D (SKQH), L326D (SKQI), E242Q (SSYU), N240D (SSYV), Q233E (SSYW), D141A/Q233E (SKQ3), D141A/Q233E/N240D (SKQ7), and Q233E/N240D (SKQK).

Acetate Activates Catalase Activity. The pH profile of catalase activity of catalase-peroxidases with a broad maximum around pH 6.5 differs from the even broader and very flat plateau of monofunctional catalases.¹⁹ The determination of pH profiles usually demands the use of several different buffers to span the pH range of 4–10, and the transition between buffers was accompanied by discontinuities in the activity profile. The discontinuities were eliminated by using a mixture of phosphate

Table 1. Data Collection and Refinement Statistics of Various BpKatG Variants

PDB entry variant	Data Collection							
	SKQ0 A290D	SKQ2 A357D	SKQ3 D141A/Q233E	SKQ6 A359D	5V53 D141A/Q233E/N240D with 25 mM acetate	5KQH V293D	5KQI L326D	5KQK Q233E/N240D
unit cell parameters								
space group	$P2_12_12_1$	$P2_12_12_1$	$P2_12_12_1$	$P2_12_12_1$	$P2_12_12_1$	$P2_12_12_1$	$P2_12_12_1$	$P2_12_12_1$
<i>a</i> (Å)	100.76	100.83	101.04	100.58	100.84	100.79	100.72	100.72
<i>b</i> (Å)	113.49	114.13	114.03	115.79	115.82	113.43	115.23	115.05
<i>c</i> (Å)	174.51	174.99	174.51	174.73	174.77	174.68	174.54	174.51
α, β, γ (deg)	90	90	90	90	90	90	90	90
resolution ^a (Å)	47.57–1.80 (1.90–1.80)	47.80–1.90 (2.00–1.80)	47.76–1.85 (1.95–1.85)	48.33–1.62 (1.71–1.62)	48.27–1.70 (1.79–1.70)	47.57–1.82 (1.92–1.87)	48.42–1.87 (1.97–1.87)	48.39–1.75 (1.84–1.75)
no. of unique reflections	181938 (26569)	154155 (22788)	152779 (23222)	251711 (35905)	214623 (32021)	178897 (25932)	165881 (24178)	199866 (29240)
completeness (%)	98.7 (99.5)	97.3 (99.3)	89.3 (93.5)	97.7 (96.3)	96.1 (98.7)	99.9 (100.0)	98.9 (99.8)	98.4 (99.2)
R_{merge}	0.059 (0.474)	0.070 (0.474)	0.076 (0.487)	0.044 (0.520)	0.061 (0.538)	0.071 (0.475)	0.092 (0.478)	0.062 (0.413)
R_{pim}	0.041 (0.330)	0.047 (0.326)	0.042 (0.283)	0.022 (0.268)	0.034 (0.310)	0.038 (0.256)	0.050 (0.256)	0.044 (0.298)
$\langle I/\sigma I \rangle$	12.3 (2.4)	10.6 (2.3)	9.8 (2.3)	20.8 (2.7)	11.7 (2.4)	14.2 (3.0)	9.3 (2.6)	12.8 (3.0)
$CC_{1/2}$	0.998 (0.811)	0.998 (0.784)	0.998 (0.802)	0.999 (0.832)	0.998 (0.814)	0.998 (0.794)	0.992 (0.808)	0.997 (0.819)
multiplicity	2.9 (2.9)	2.9 (2.9)	3.7 (3.6)	4.7 (4.2)	3.9 (3.8)	4.3 (4.4)	4.1 (4.2)	2.7 (2.7)
	Model Refinement							
no. of reflections	172743	146428	145121	238907	203772	169937	157637	189792
R_{cryst} (%)	15.2	15.6	15.9	14.5	14.3	15.4	16.4	15.2
R_{free} (%)	18.5	19.1	19.5	17.0	17.2	18.4	19.8	18.2
no. of non-H atoms	12876	12676	12481	12835	12697	12795	12535	12860
no. of water molecules	1625	1425	1255	1579	1465	1550	1271	1629
average <i>B</i> factor (Å ²)								
protein	24.4	27.0	28.3	23.2	25.3	22.1	27.5	20.1
heme	17.2	20.6	21.3	16.4	18.9	15.4	20.4	13.1
waters	33.8	34.9	35.1	32.9	33.9	31.7	34.3	29.4
other								
coordinate error (Å) ^b	0.073	0.089	0.086	0.048	0.052	0.072	0.088	0.066
root-mean-square deviation for bonds (Å)	0.028	0.023	0.023	0.034	0.028	0.027	0.028	0.028
root-mean-square deviation for angles (deg)	2.27	2.03	2.01	2.66	2.29	2.26	2.32	2.23

Table 1. continued

PDB entry variant	Data Collection			
	SKSF	STXQ	SKSK	SSYU
D141A with 25 mM acetate	A143D	5TYQ	native with 50 mM acetate	SSYU
D141A/Q233E/N240D				E242Q
SV40				N240D
5SYW				SSYU
Q233E				N240D
5V40				SSYU
D141A/Q233E/N240D				SSYU
unit cell parameters				SSYU
space group	$P2_12_12_1$	$P2_12_12_1$	$P2_12_12_1$	$P2_12_12_1$
a (Å)	100.69	100.67	100.71	100.82
b (Å)	115.47	115.18	115.48	113.71
c (Å)	174.59	174.74	174.97	174.62
α, β, γ (deg)	90	90	90	90
resolution ^a (Å)	48.37–1.75 (1.84–1.75)	48.37–1.90 (2.00–1.90)	48.39–1.69 (1.78–1.69)	57.08–1.80 (1.90–1.80)
no. of unique reflections	203501 (29608)	159525 (22983)	225720 (32915)	166673 (24661)
completeness (%)	99.6 (99.9)	99.8 (99.6)	99.4 (99.8)	90.3 (92.2)
R_{merge}	0.062 (0.481)	0.077 (0.563)	0.070 (0.484)	0.095 (0.457)
R_{pim}	0.030 (0.235)	0.038 (0.276)	0.040 (0.291)	0.052 (0.251)
$\langle I/\sigma I \rangle$	14.7 (3.1)	17.5 (2.9)	10.8 (2.4)	8.3 (2.7)
$CC_{1/2}$	0.998 (0.872)	0.998 (0.824)	0.996 (0.807)	0.994 (0.819)
multiplicity	4.9 (5.0)	5.0 (5.0)	3.7 (3.7)	3.8 (3.5)
no. of reflections	193124	151540	214411	157558
R_{cyst} (%)	14.8	15.7	15.2	13.9
R_{free} (%)	17.5	19.1	18.0	17.2
no. of non-H atoms	12667	12726	12836	12746
no. of water molecules	1439	1683	1608	1507
average B factor (Å ²)				
protein	27.4	26.3	25.3	21.9
heme	21.0	20.2	18.6	15.0
waters	35.3	33.8	34.3	30.7
other				
coordinate error (Å) ^b	0.060	0.088	0.058	0.058
root-mean-square deviation for bonds (Å)	0.031	0.027	0.030	0.027
root-mean-square deviation for angles (deg)	2.44	2.22	2.40	2.27
5SYW				SSYU
Q233E				N240D
5V40				SSYU
D141A/Q233E/N240D				N240D
5SYW				SSYU
Q233E				N240D
5V40				SSYU
D141A/Q233E/N240D				N240D
5SYW				SSYU
Q233E				N240D
5V40				SSYU
D141A/Q233E/N240D				N240D
5SYW				SSYU
Q233E				N240D
5V40				SSYU
D141A/Q233E/N240D				N240D
5SYW				SSYU
Q233E				N240D
5V40				SSYU
D141A/Q233E/N240D				N240D
5SYW				SSYU
Q233E				N240D
5V40				SSYU
D141A/Q233E/N240D				N240D
5SYW				SSYU
Q233E				N240D
5V40				SSYU
D141A/Q233E/N240D				N240D
5SYW				SSYU
Q233E				N240D
5V40				SSYU
D141A/Q233E/N240D				N240D
5SYW				SSYU
Q233E				N240D
5V40				SSYU
D141A/Q233E/N240D				N240D
5SYW				SSYU
Q233E				N240D
5V40				SSYU
D141A/Q233E/N240D				N240D
5SYW				SSYU
Q233E				N240D
5V40				SSYU
D141A/Q233E/N240D				N240D
5SYW				SSYU
Q233E				N240D
5V40				SSYU
D141A/Q233E/N240D				N240D
5SYW				SSYU
Q233E				N240D
5V40				SSYU
D141A/Q233E/N240D				N240D
5SYW				SSYU
Q233E				N240D
5V40				SSYU
D141A/Q233E/N240D				N240D
5SYW				SSYU
Q233E				N240D
5V40				SSYU
D141A/Q233E/N240D				N240D
5SYW				SSYU
Q233E				N240D
5V40				SSYU
D141A/Q233E/N240D				N240D
5SYW				SSYU
Q233E				N240D
5V40				SSYU
D141A/Q233E/N240D				N240D
5SYW				SSYU
Q233E				N240D
5V40				SSYU
D141A/Q233E/N240D				N240D
5SYW				SSYU
Q233E				N240D
5V40				SSYU
D141A/Q233E/N240D				N240D
5SYW				SSYU
Q233E				N240D
5V40				SSYU
D141A/Q233E/N240D				N240D
5SYW				SSYU
Q233E				N240D
5V40				SSYU
D141A/Q233E/N240D				N240D
5SYW				SSYU
Q233E				N240D
5V40				SSYU
D141A/Q233E/N240D				N240D
5SYW				SSYU
Q233E				N240D
5V40				SSYU
D141A/Q233E/N240D				N240D
5SYW				SSYU
Q233E				N240D
5V40				SSYU
D141A/Q233E/N240D				N240D
5SYW				SSYU
Q233E				N240D
5V40				SSYU
D141A/Q233E/N240D				N240D
5SYW				SSYU
Q233E				N240D
5V40				SSYU
D141A/Q233E/N240D				N240D
5SYW				SSYU
Q233E				N240D
5V40				SSYU
D141A/Q233E/N240D				N240D
5SYW				SSYU
Q233E				N240D
5V40				SSYU
D141A/Q233E/N240D				N240D
5SYW				SSYU
Q233E				N240D
5V40				SSYU
D141A/Q233E/N240D				N240D
5SYW				SSYU
Q233E				N240D
5V40				SSYU
D141A/Q233E/N240D				N240D
5SYW				SSYU
Q233E				N240D
5V40				SSYU
D141A/Q233E/N240D				N240D
5SYW				SSYU
Q233E				N240D
5V40				SSYU
D141A/Q233E/N240D				N240D
5SYW				SSYU
Q233E				N240D
5V40				SSYU
D141A/Q233E/N240D				N240D
5SYW				SSYU
Q233E				N240D
5V40				SSYU
D141A/Q233E/N240D				N240D
5SYW				SSYU
Q233E				N240D
5V40				SSYU
D141A/Q233E/N240D				N240D
5SYW				SSYU
Q233E				N240D
5V40				SSYU
D141A/Q233E/N240D				N240D
5SYW				SSYU
Q233E				N240D
5V40				SSYU
D141A/Q233E/N240D				N240D
5SYW				SSYU
Q233E				N240D
5V40				SSYU
D141A/Q233E/N240D				N240D
5SYW				SSYU
Q233E				N240D
5V40				SSYU
D141A/Q233E/N240D				N240D
5SYW				SSYU
Q233E				N240D
5V40				SSYU
D141A/Q233E/N240D				N240D
5SYW				SSYU
Q233E				N240D
5V40				SSYU
D141A/Q233E/N240D				N240D
5SYW				SSYU
Q233E				N240D
5V40				SSYU
D141A/Q233E/N240D				N240D
5SYW				SSYU
Q233E				N240D
5V40				SSYU
D141A/Q233E/N240D				N240D
5SYW				SSYU
Q233E				N240D
5V40				SSYU
D141A/Q233E/N240D				N240D
5SYW				SSYU
Q233E				N240D
5V40				SSYU
D141A/Q233E/N240D				N240D
5SYW				SSYU
Q233E				N240D
5V40				SSYU
D141A/Q233E/N240D				N240D
5SYW				SSYU
Q233E				N240D
5V40				SSYU
D141A/Q233E/N240D				N240D
5SYW				SSYU
Q233E				N240D
5V40				SSYU
D141A/Q233E/N240D				N240D
5SYW				SSYU
Q233E				N240D
5V40				SSYU
D141A/Q233E/N240D				N240D
5SYW				SSYU
Q233E				N240D
5V40				SSYU
D141A/Q233E/N240D				N240D
5SYW				SSYU
Q233E				N240D
5V40				SSYU
D141A/Q233E/N240D				N240D
5SYW				SSYU
Q233E				N240D
5V40				SSYU
D141A/Q233E/N240D				N240D
5SYW				SSYU
Q233E				N240D
5V40				SSYU
D141A/Q233E/N240D				N240D
5SYW				SSYU
Q233E				N240D
5V40				SSYU
D141A/Q233E/N240D				N240D
5SYW				SSYU
Q233E				N240D
5V40				SSYU
D141A/Q233E/N240D				N240D
5SYW				SSYU
Q233E				N240D
5V40				SSYU
D141A/Q233E/N240D				N240D
5SYW				SSYU
Q233E				N240D
5V40				

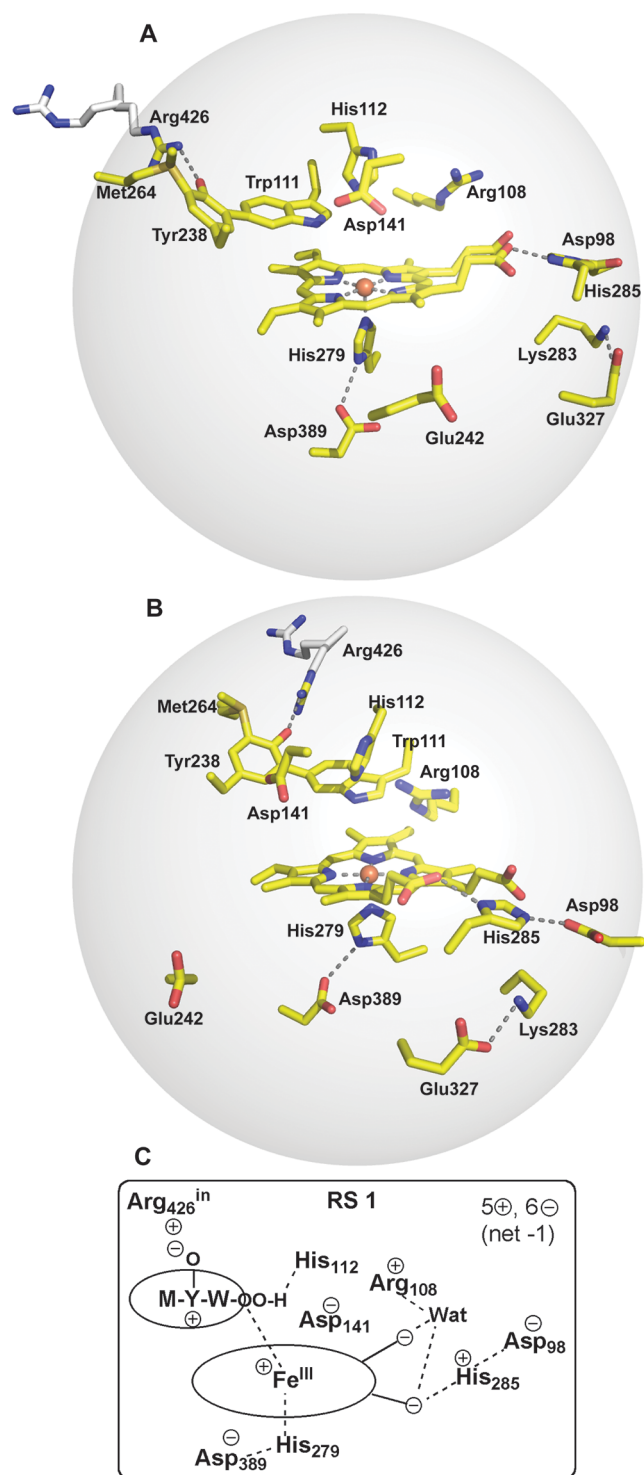


Figure 4. Location of protonable residues within a 15 Å radius of the heme iron. Panel B is rotated approximately 90° compared to panel A. In panel C, the charges in the vicinity of the heme in RS 1 illustrate the net negative charge of the region.

and acetate across the whole pH range, revealing a 10–15% increase in the catalase activity of native BpKatG at pH 6.5, and even more strikingly a 10-fold increase in the catalase activity of the D141A variant at pH 5.0 compared to those for buffers without acetate present (Table 2 and Figure 5). The pH optima of both enzymes appear to be unchanged by the acetate, pH 6.5 for the native enzyme and pH 5.0 for D141A (Figure 5A), although the very low activity of D141A in the absence of acetate

Table 2. Catalase and Peroxidase Activities of BpKatG Variants

variant	catalase ^a [$\mu\text{mol of H}_2\text{O}_2$ ($\mu\text{mol of heme})^{-1} \text{s}^{-1}$]	peroxidase ^b [$\mu\text{mol of ABTS}$ ($\mu\text{mol of heme})^{-1} \text{s}^{-1}$]
WT	9450 ± 520	19.3 ± 0.3
WT with acetate	10500 ± 430	19.3 ± 0.3
WT with formate	10300 ± 420	nd ^c
WT with propionate	10130 ± 390	nd ^c
A143D	17660 ± 630	13.9 ± 0.2
L209D	11010 ± 90	16.2 ± 0.4
E210Q	7730 ± 320	16.3 ± 0.3
L211D	10370 ± 380	19.2 ± 0.3
Q233E	17530 ± 740	17.6 ± 0.3
L236D	6560 ± 120	6.3 ± 0.1
N240D	18990 ± 780	21.0 ± 0.4
E242Q	1380 ± 40	12.5 ± 0.3
A290D	6410 ± 180	11.2 ± 0.2
V293D	14260 ± 620	18.3 ± 0.2
E296A	5990 ± 230	16.9 ± 0.2
L326D	6706 ± 280	17.6 ± 0.3
A357D	12130 ± 350	14.0 ± 0.2
A359D	14570 ± 150	17.5 ± 0.3
Q233E/N240D	18920 ± 550	19.8 ± 0.2
D141E	5910 ± 160	18.2 ± 0.2
D114N	1060 ± 50	13.7 ± 0.2
D141A	420 ± 30	16.4 ± 0.2
D141A/Q233E	533 ± 30	18.7 ± 0.4
D141A/Q233E/N240D	530 ± 20	15.8 ± 0.2
D141A with acetate ^d	5840 ± 180	16.4 ± 0.2
D141A with formate ^d	1550 ± 110	nd ^c
D141A with propionate ^d	2860 ± 210	nd ^c

^aCatalase activity was determined at pH 7.0 with 60 mM H₂O₂. ^bPeroxidase activity was determined at pH 4.5 with 2.5 mM H₂O₂ and 0.4 mM ABTS. ^cNot determined. ^dAcetate, formate, and propionate at 50 mM.

(plotted on a separate axis with a dashed line in Figure 5A) appears to plateau at lower pHs. For comparison, the optimal pHs for E240Q and N240D are 5.5 and 7.0, respectively. The apparent K_M values of BpKatG for H₂O₂ are unchanged by acetate from those reported previously (25 mM at pH 6.5 and 62 mM at pH 5.0).¹⁹ D141A differed slightly in acetate, its apparent K_M for H₂O₂ decreasing from 65 to 30 mM at both pH 5.0 and 6.5. Formate and propionate also at 50 mM induce smaller increases in the activity of D141A (Table 2), leading to the conclusion that carboxylate-containing molecules external to the protein can also enhance the catalase reaction.

To investigate if acetate binds to the protein, crystals of the native enzyme and the D141A variant were grown in the presence of 50 and 25 mM acetate, respectively, and X-ray diffraction data sets were collected. The electron density maps of the native enzyme contain no evidence of acetate binding anywhere on the protein (SKSK), whereas the maps of the D141A variant contain new regions of density, well satisfied by acetate, deep in the heme cavity, associated with the heme iron, distal Trp₁₁₁ and His₁₁₂ (Figure 6 and SKSF). Acetate was also found in a similar location in the heme cavity of triple variant D141A/Q233E/N240D (SV53). Thus, acetate enters the access channel and heme cavity in the absence of Asp₁₄₁, and its presence facilitates the catalase reaction.

Entrance Channel Carboxylates Influence M-Y-W₁₁₁-OOH. The perhydroxy modification, M-Y-W₁₁₁-OOH, is found

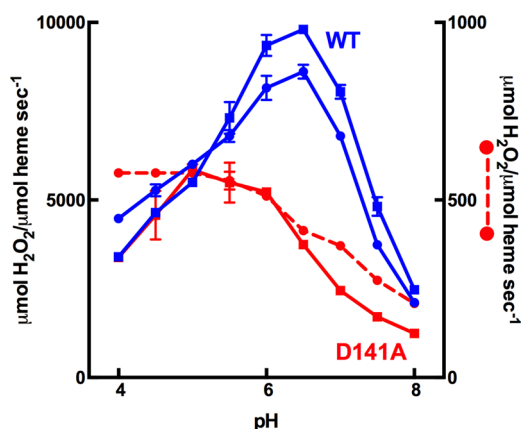


Figure 5. Effect of acetate on the catalase activity of WT BpKatG (blue) and its D141A variant (red). The catalase activity was determined without (filled circles) and with (filled squares) 50 mM sodium acetate added to the buffer. The activity of D141A is ~10% of the activity with acetate present and is plotted using a dashed line and the right axis. Error bars are shown for all points but in some cases are not visible because they are smaller than the size of the marker.

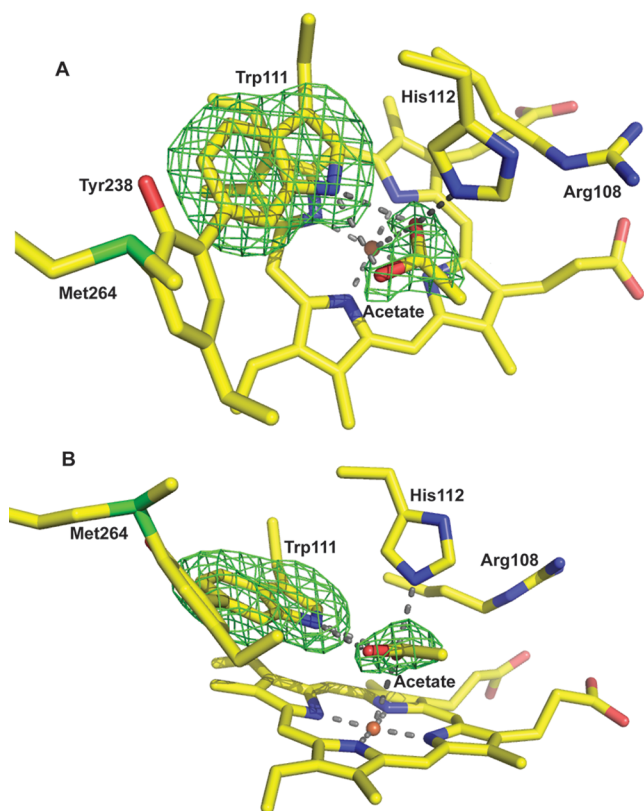


Figure 6. Two views of acetate bound in the heme cavity of D141A. The $F_o - F_c$ omit electron density maps at 7.0σ were calculated without Trp₁₁₁ or acetate in the model.

in the native enzyme at pH 6.1 with ~60% occupancy split in two orientations. The predominant A orientation in the native enzyme and most variants is hydrogen bonded with the imidazole of His₁₁₂ (Figure 1); the less common B orientation is rotated ~180° from His₁₁₂ (Figure 1). Removing the carboxylate of Asp₁₄₁ (in D141A) causes a dramatic change in the orientation of the perhydroxy modification from a predominantly A orientation to a predominantly B orientation,⁸ but with similar ~60% occupancy (5SYH), suggesting a correlation

between the B orientation and the inactivity of D141A.⁸ However, the introduction of a channel carboxylate into the double and triple variants, D141A/Q233E (SKQ3) and D141A/Q233E/N240D (SV53), respectively, led to an increase in the A orientation, but without an increase in activity.

Computation of pK_a s of Protonable Side Chains in BpKatG. To understand more clearly the interplay between Asp₁₄₁ and Arg₁₀₈, wherein both must be present or absent for catalase activity, and the impact of the channel carboxylates on charged residues in the vicinity of the heme, the pK_a s of ionizable residues in the 15 Å sphere centered on the heme iron (Figure 4) were computed looking, in addition, at the influence of externally added acetate, the perhydroxy modification on the M-Y-W adduct (M-Y-W₁₁₁-OOH), the mobile Arg₄₂₆, and conversion to Cpd I (Table 3). Remarkably, the only residue in the heme cavity

Table 3. Computed pK_a Values for Selected Protonable Groups in BpKatG and Selected Variants

variant	MYW-OOH conformation	His ₁₁₂	Asp ₁₄₁	Asp ₃₈₉	Glu ₂₄₂	PD ^a
E242Q	A	5.8	<0 ^b	<0	—	1.1
WT RS 1	A	6.2	<0	<0	3.0	1.1
Q233E	A	6.6	<0	<0	3.1	1.1
N240D	A	6.7	<0	<0	3.8	1.2
E242Q	B	6.6	<0	<0	—	1.1
WT RS 1	B	7.0	<0	<0	3.0	1.1
Q233E	B	7.5	<0	<0	3.1	1.2
N240D	B	7.5	<0	<0	3.8	1.3
D141A with acetate	—	8.9	—	<0	2.7	2.3
D141A with acetate at 2.5 Å	—	8.2	—	<0	2.9	2.2
D141A with acetate at 5.0 Å	—	7.0	—	<0	3.1	1.9
D141A with acetate at 7.5 Å	—	5.8	—	<0	2.8	1.0
D141A (no acetate)	B	4.6	—	<0	2.2	0.4
R108A	B	9.6	<0	<0	3.3	3.6
D141A/R108A	B	7.3	—	<0	2.7	2.8
WT RS 2 Y ₂₃₈ -O ⁻	—	7.8	<0	<0	3.0	1.6
WT RS 2 Y ₂₃₈ -O ⁻ +R ₄₂₆	—	7.2	<0	<0	2.9	1.3
WT RS 2 Y ₂₃₈ -OH	—	6.1	<0	<0	2.8	1.0
Cpd I D141A	—	6.3	—	<0	2.5	2.3
Cpd I E242Q	—	8.5	<0	<0	—	2.9
WT Cpd I	—	8.9	<0	<0	3.2	3.1
Cpd I Q233E	—	9.3	<0	<0	3.2	3.1
Cpd I N240D	—	9.3	<0	<0	3.7	3.1
Cpd I D141A/Q233E	—	6.5	—	<0	2.7	2.4
Cpd I D141A/N240D	—	6.6	—	<0	3.7	2.4

^aPD, heme propionate D. ^bThe reported values of <0 correspond to those of acidic residues that have their charged species stabilized by a nearby positively charged residue and should be interpreted as nontitrable in the physiological pH range.

that exhibits a change in pK_a within the pH range of catalase activity (pH 4.0–8.0) in response to changes in nearby residues is His₁₁₂, and the changes are substantial from 4.6 in D141A to 9.6 in R108A (Figure 7 and Table 3). Within this range, the pK_a of His₁₁₂ is very sensitive to its surrounding electrostatic environment being influenced by M-Y-W₁₁₁-OOH, by the orientation of Arg₄₂₆, by the protonation of Y₂₃₈, and by carboxylates in the entrance channel.

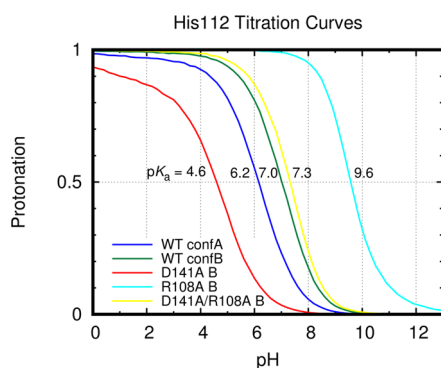


Figure 7. Titration curves of His₁₁₂ in different variants of BpKatG, including the pK_a values determined for each. conf A and conf B refer to the two orientations of the perhydroxy modification on W₁₁₁ (Figure 1).

Protonation of His₁₁₂ is precluded by its hydrogen bonding interaction with M-Y-W₁₁₁-OOH in the A orientation, and the pK_a values reported are generally for M-Y-W₁₁₁-OOH in the B orientation, for example, 7.0 in the native enzyme with Arg₄₂₆ in ionic contact with Tyr₂₃₈. Removal of the perhydroxy from M-Y-W₁₁₁-OOH (as O₂ or superoxide after INH treatment) and the shift of Arg₄₂₆ to the out conformation increase the pK_a of His₁₁₂ to 7.8, and protonation of Tyr₂₃₈ lowers it to 6.1 (Table 3). Conversion of the heme iron of native BpKatG to an oxo-ferryl species introduces an electronegative atom (oxygen) next to His₁₁₂, which increases its pK_a to 8.9, which is consistent with the reported increase in the pK_a of the distal His in Cpd I of *Coprinus cinereus* peroxidase.⁴¹

Arguably, the most striking correlation is between catalase activity and changes in the His₁₁₂ pK_a of both the resting state and Compound I species in the series of variants D141A, E242Q, native BpKatG, and N240D wherein the resting state pK_a of His₁₁₂ changes from 4.6 to 6.6 to 7.0 to 7.5 and the Compound I pK_a of His₁₁₂ changes from 6.3 to 8.5 to 8.9 to 9.3 as the catalase activity increases from 0.05 to 0.15 to 1.0 to 2.0 times the native level, respectively (Table 3). A similar correlation is evident in the increase in the catalase activity of D141A from 0.5 to 0.5 of native levels caused by acetate and the calculated pK_a of His₁₁₂ that increases from 4.6 to 8.2 as acetate is moved progressively closer to the heme (Table 3). Similarly, the single variants, D141A and R108A, have low activity (0.05 and 0.10 of native levels, respectively) correlated with extreme pK_a values (4.6 and 9.6, respectively), whereas double variant D141A/R108A with 0.8 of native activity has a pK_a of 7.3.

DISCUSSION

Considerable progress has been made in our understanding of the mechanism underlying the catalase reaction in catalase-peroxidases, but the basis for how distant charged species and acetate in the buffer can influence the catalase reaction, but not the peroxidase reaction, still lacks a clear explanation. The hypothesis pursued in this work is that the influence of remote negative charges is mediated through a charged or protonable species in the vicinity of the heme. Protonable species include Arg₁₀₈, His₁₁₂, Asp₁₄₁, Trp₁₁₁, and Y₂₃₈, and the M-Y-W adduct, as a whole, may carry a positive charge while interacting with the mobile Arg₄₂₆ and as the transient radical in the catalytic cycle (Figure 2). However, the direct involvement of Arg₁₀₈ and Asp₁₄₁ can be eliminated by the observation that double variant D141A/R108A, lacking both side chains, exhibits near normal catalase activity. Similarly, an increased level of protonation of

Tyr₂₃₈ would weaken its interaction with Arg₄₂₆, essential for catalase activity, and more difficult deprotonation of Trp₁₁₁ would interfere with the process of Compound I reduction. Therefore, by a process of elimination, His₁₁₂ and the M-Y-W adduct are the most likely candidates to mediate remote charge effects.

To test the hypothesis that His₁₁₂ might be responding to remote negative charges, the pK_as of all protonable residues near the heme were computed, revealing that only His₁₁₂ responds to environmental changes in the pH range of catalase activity. The resting state pK_a of His₁₁₂ of 7.0 (with M-Y-W₁₁₁-H) is higher than expected for a normal histidine, consistent with the predicted negative electrostatic environment in the heme cavity (Figure 4C). Significantly, there is a correlation of increasing His₁₁₂ pK_as in the narrow range of 6.5 and 7.5 with increasing catalase activity and with increasing numbers of channel carboxylates. Removal of either Arg₁₀₈ or especially Asp₁₄₁ close to His₁₁₂ causes more extreme changes in His₁₁₂ pK_a outside of the normal activity pH range of the native enzyme, for example 4.6 in D141A and 9.6 in R108A, and these changes are associated with greatly decreased catalase activity. A similar correlation is also evident among the Compound I species of the variants ranging from 6.3 to 9.3. The optimal pHs of the catalase reactions of the variants are also correlated with the pK_a of His₁₁₂. The involvement of a protonated histidine is also consistent with the more rapid disappearance of catalase activity above pH 8 than below pH 6.¹⁹

What then is the role of protonated His₁₁₂? At pH 6.5, the optimum for catalase activity of native BpKatG, >80% of the M-Y-W adduct has the perhydroxy modification (M-Y-W₁₁₁-OOH) hydrogen bonded to His₁₁₂ (RS 1 in Figure 2A),⁴² precluding its protonation. However, RS 1 and RS 2 are in equilibrium, and increases in the pK_a of His₁₁₂ will shift the protonation equilibrium of RS 2 (Figure 2) toward the more protonated species, which, in turn, will pull the resting state equilibrium toward RS 2 required for continuation of the catalase reaction cycle (Figure 2). The fact that RS 1 predominates in a catalytically active crystal suggests that it is at an energy minimum in the reaction pathway and anything that facilitates the release of O₂ and the conversion of RS 1 to RS 2, including enhanced protonation of His₁₁₂, will enhance this step of the catalase reaction. The large variations in the pK_a of His₁₁₂ in Compound I suggest that protonated His₁₁₂ may also be a key determinant in the catalytic reduction of Compound I by the second H₂O₂ molecule (Figure 2).

The very low catalase activity of D141A, which is unaffected by carboxylates in the channel, is relatively insensitive to pH but is activated by acetate (Figure 5), which seems to suggest that, besides protonation of His₁₁₂, the stability of a charged species is critical to the catalase cycle. A likely candidate is the transient adduct cation radical formed during Compound I reduction (Figure 2), which would be less stable with a less electronegative potential as in D141A and more stable with acetate present.

In summary, the catalase activity of catalase-peroxidases is dependent on a negative electrostatic potential in the vicinity of the heme, which is enhanced by carboxylate side chains in the entrance channel and by acetate approaching the heme. The negative potential influences catalase activity by modulating the pK_a of His₁₁₂ and by stabilizing the transient charged M-Y-W adduct radical that is integral to the catalase reaction.

■ AUTHOR INFORMATION

Corresponding Author

*Phone: 204-797-2134. E-mail: peter.loewen@umanitoba.ca.

ORCID 

Miguel Machuqueiro: 0000-0001-6923-8744

Carne Rovira: 0000-0003-1477-5010

Peter C. Loewen: 0000-0003-4507-4356

Funding

This work was supported by a Discovery Grant 9600 from the Natural Sciences and Engineering Research Council (NSERC) of Canada (to P.C.L.) and the Canada Research Chair Program (to P.C.L.). The Canadian Light Source is supported by the Natural Sciences and Engineering Research Council of Canada, the National Research Council Canada, the Canadian Institutes of Health Research, the Province of Saskatchewan, Western Economic Diversification Canada, and the University of Saskatchewan. We also acknowledge financial support from the Portuguese Fundação para a Ciência e a Tecnologia through Project UID/MULTI/00612/2013.

Notes

The authors declare no competing financial interest.

■ REFERENCES

- (1) Claiborne, A., and Fridovich, I. (1979) Purification of the o-dianisidine peroxidase from *Escherichia coli* B. Physicochemical characterization and analysis of its dual catalytic and peroxidatic activities. *J. Biol. Chem.* 254, 4245–4252.
- (2) Shoeb, H. A., Bowman, B. U., Jr., Ottolenghi, A. C., and Merola, A. J. (1985) Peroxidase-mediated oxidation of isoniazid. *Antimicrob. Agents Chemother.* 27, 399–403.
- (3) Shoeb, H. A., Bowman, B. U., Jr., Ottolenghi, A. C., and Merola, A. J. (1985) Evidence for the generation of active oxygen by isoniazid treatment of extracts of *Mycobacterium tuberculosis* H37Ra. *Antimicrob. Agents Chemother.* 27, 404–407.
- (4) Shoeb, H. A., Bowman, B. U., Jr., Ottolenghi, A. C., and Merola, A. J. (1985) Enzymatic and nonenzymatic superoxide-generating reactions of isoniazid. *Antimicrob. Agents Chemother.* 27, 408–412.
- (5) Zhang, Y., Heym, B., Allen, B., Young, D., and Cole, S. (1992) The catalase-peroxidase gene and isoniazid resistance of *Mycobacterium tuberculosis*. *Nature* 358, 591–593.
- (6) Vidossich, P., Alfonso-Prieto, M., Carpena, X., Loewen, P. C., Fita, I., and Rovira, C. (2007) Versatility of the electronic structure of compound I in catalase-peroxidases. *J. Am. Chem. Soc.* 129, 13436–13446.
- (7) Vidossich, P., Carpena, X., Loewen, P. C., Fita, I., and Rovira, C. (2011) Oxygen binding to catalase-peroxidase. *J. Phys. Chem. Lett.* 2, 196–200.
- (8) Loewen, P. C., Carpena, X., Vidossich, P., Fita, I., and Rovira, C. (2014) An ionizable active-site tryptophan imparts catalase activity to a peroxidase core. *J. Am. Chem. Soc.* 136, 7249–7252.
- (9) Colin, J., Wiseman, B., Switala, J., Loewen, P. C., and Ivancich, A. (2009) Distinct role of specific tryptophans in facilitating electron transfer or as [Fe(IV)=O Trp(*)] intermediates in the peroxidase reaction of *Burkholderia pseudomallei* catalase-peroxidase. *J. Am. Chem. Soc.* 131, 8557–8563.
- (10) Wiseman, B., Carpena, X., Feliz, M., Donald, L. J., Pons, M., Fita, I., and Loewen, P. C. (2010) Isonicotinic acid hydrazide conversion to isonicotinyl-NAD by catalase-peroxidases. *J. Biol. Chem.* 285, 26662–26673.
- (11) Vlasits, J., Jakopitsch, C., Bernroither, M., Zamocky, M., Furtmüller, P. G., and Obinger, C. (2010) Mechanisms of catalase activity of heme peroxidases. *Arch. Biochem. Biophys.* 500, 74–81.
- (12) Zhao, X., Suarez, J., Khajo, A., Yu, S., Metlitsky, L., and Magliozzo, R. S. (2010) A radical on the Met-Tyr-Trp modification required for catalase activity in catalase-peroxidase is established by isotopic labeling and site-directed mutagenesis. *J. Am. Chem. Soc.* 132, 8268–8269.
- (13) Jakopitsch, C., Auer, M., Regelsberger, G., Jantschko, W., Furtmüller, P. G., Ruker, F., and Obinger, C. (2003) Distal site aspartate is essential in the catalase activity of catalase-peroxidases. *Biochemistry* 42, 5292–5300.
- (14) Deemagarn, T., Wiseman, B., Carpena, X., Ivancich, A., Fita, I., and Loewen, P. C. (2007) Two alternative substrate paths for compound I formation and reduction in catalase-peroxidase KatG from *Burkholderia pseudomallei*. *Proteins: Struct., Funct., Genet.* 66, 219–228.
- (15) Jakopitsch, C., Droghetti, E., Schmuckenschlager, F., Furtmüller, P. G., Smulevich, G., and Obinger, C. (2005) Role of the main access channel of catalase-peroxidase in catalysis. *J. Biol. Chem.* 280, 42411–42422.
- (16) Chelikani, P., Carpena, X., Fita, I., and Loewen, P. C. (2003) An electrical potential in the access channel of catalases enhances catalysis. *J. Biol. Chem.* 278, 31290–31296.
- (17) Rørth, M., and Jensen, P. K. (1967) Determination of catalase activity by means of the Clark oxygen electrode. *Biochim. Biophys. Acta* 139, 171–173.
- (18) Childs, R. E., and Bardsley, W. G. (1975) The steady-state kinetics of peroxidase with 2,2'-azino-di-(3-ethylbenzthiazoline-6-sulphonic acid) as chromogen. *Biochem. J.* 145, 93–103.
- (19) Singh, R., Wiseman, B., Deemagarn, T., Jha, V., Switala, J., and Loewen, P. C. (2008) Comparative study of catalase-peroxidases (KatGs). *Arch. Biochem. Biophys.* 471, 207–214.
- (20) Kunkel, T. A., Roberts, J. D., and Zakour, R. A. (1987) Rapid and efficient site specific mutagenesis without phenotypic selection. *Methods Enzymol.* 154, 367–382.
- (21) Carpena, X., Loprasert, S., Mongkolsuk, S., Switala, J., Loewen, P. C., and Fita, I. (2003) Catalase-peroxidase KatG of *Burkholderia pseudomallei* at 1.7 Å resolution. *J. Mol. Biol.* 327, 475–489.
- (22) Kabsch, W. (2010) XDS. *Acta Crystallogr., Sect. D: Biol. Crystallogr.* 66, 125–132.
- (23) Winn, M. D., Ballard, C. C., Cowtan, K. D., Dodson, E. J., Emsley, P., Evans, P. R., Keegan, R. M., Krissinel, E. B., Leslie, A. G. W., McCoy, A., McNicholas, S. J., Murshudov, G. N., Pannu, N. S., Potterton, E. A., Powell, H. R., Read, R. J., Vagin, A., and Wilson, K. S. (2011) Overview of the CCP4 suite and current developments. *Acta Crystallogr., Sect. D: Biol. Crystallogr.* 67, 235–242.
- (24) Murshudov, G. N., Vagin, A. A., and Dodson, E. J. (1997) Refinement of macromolecular structures by the maximum-likelihood method. *Acta Crystallogr., Sect. D: Biol. Crystallogr.* 53, 240–255.
- (25) Emsley, P., Lohkamp, B., Scott, W. G., and Cowtan, K. (2010) Features and development of Coot. *Acta Crystallogr., Sect. D: Biol. Crystallogr.* 66, 486–501.
- (26) Ho, B. K., and Gruswitz, F. (2008) HOLLOW: generating accurate representations of channel and interior surfaces in molecular structures. *BMC Struct. Biol.* 8, 49–54.
- (27) Carpena, X., Wiseman, B., Deemagarn, T., Singh, R., Switala, J., Ivancich, A., Fita, I., and Loewen, P. C. (2005) A molecular switch and electronic circuit modulate catalase activity in catalase-peroxidases. *EMBO Rep.* 6, 1156–1162.
- (28) Vidossich, P., Loewen, P. C., Carpena, X., Fiorin, G., Fita, I., and Rovira, C. (2014) Binding of antitubercular pro-drug isoniazid in the heme access channel of catalase peroxidase (KatG). A combined structural and metadynamics investigation. *J. Phys. Chem. B* 118, 2924–2931.
- (29) Deemagarn, T., Carpena, X., Singh, R., Wiseman, B., Fita, I., and Loewen, P. C. (2005) Structural characterization of the Ser324Thr variant of the catalase-peroxidase (KatG) from *Burkholderia pseudomallei*. *J. Mol. Biol.* 345, 21–28.
- (30) Teixeira, V. H., Ventura, C., Leitão, R., Ráfols, C., Bosch, E., Martins, F., and Machuqueiro, M. (2015) Molecular details of INH-C10 binding to wt KatG and its S315T mutant. *Mol. Pharmaceutics* 12, 898–909.

(31) Chai, J.-D., and Head-Gordon, M. (2008) Systematic optimization of long-range corrected hybrid density functionals. *J. Chem. Phys.* 128, 084106.

(32) Schmid, N., Eichenberger, A., Choutko, A., Riniker, S., Winger, M., Mark, A., and van Gunsteren, W. (2011) Definition and testing of the GROMOS force-field versions 54A7 and 54B7. *Eur. Biophys. J.* 40, 843–856.

(33) Huang, W., Lin, Z., and van Gunsteren, W. F. (2011) Validation of the GROMOS 54A7 force field with respect to β -peptide folding. *J. Chem. Theory Comput.* 7, 1237–1243.

(34) Teixeira, V. H., Cunha, C. A., Machuqueiro, M., Oliveira, A. S. F., Victor, B. L., Soares, C. M., and Baptista, A. M. (2005) On the use of different dielectric constants for computing individual and pairwise terms in Poisson-Boltzmann studies of protein ionization equilibrium. *J. Phys. Chem. B* 109, 14691–14706.

(35) Baptista, A. M., and Soares, C. M. (2001) Some theoretical and computational aspects of the inclusion of proton isomerism in the protonation equilibrium of proteins. *J. Phys. Chem. B* 105, 293–309.

(36) Bashford, D., and Gerwert, K. (1992) Electrostatic calculations of the pK_a values of ionizable groups in bacteriorhodopsin. *J. Mol. Biol.* 224, 473–486.

(37) Bashford, D. (1997) An Object-Oriented Programming Suite for Electrostatic Effects in Biological Molecules. In *Scientific Computing in Object-Oriented Parallel Environments, ISCOPE97* (Ishikawa, Y., Oldehoeft, R. R., Reynders, J. V. W., and Tholburn, M., Eds.) Springer, Berlin.

(38) Richards, F. M. (1977) Areas, volumes, packing and protein structure. *Annu. Rev. Biophys. Bioeng.* 6, 151–176.

(39) Gilson, M. K., Sharp, K. A., and Honig, B. (1988) Calculating electrostatic interactions in biomolecules: Method and error assessment. *J. Comput. Chem.* 9, 327–335.

(40) Baptista, A. M., Martel, P. J., and Soares, C. M. (1999) Simulation of electron-proton coupling with a Monte Carlo method: application to cytochrome c3 using continuum electrostatics. *Biophys. J.* 76, 2978–2998.

(41) Abelskov, A. K., Smith, A. T., Rasmussen, C. B., Dunford, H. B., and Welinder, K. G. (1997) pH dependence and structural interpretation of the reactions of *Coprinus cinereus* peroxidase with hydrogen peroxide, ferulic acid and 2,2'-axinobis(3-ethylbenzthiazoline-6-sulfonic acid). *Biochemistry* 36, 9453–9463.

(42) Carpena, X., Wiseman, B., Deemagarn, T., Herguedas, B., Ivancich, A., Singh, R., Loewen, P. C., and Fita, I. (2006) Roles for Arg426 and Trp111 in the modulation of NADH oxidase activity of catalase-peroxidase KatG from *Burkholderia pseudomallei* inferred from pH-induced structural changes. *Biochemistry* 45, 5171–5179.